

Measurements of ${}^3_{\Lambda}\text{H}$ and ${}^4_{\Lambda}\text{H}$ Lifetimes and Yields in Au+Au Collisions in the High Baryon Density Region

M. S. Abdallah,⁵ B. E. Aboona,⁵⁵ J. Adam,⁶ L. Adamczyk,² J. R. Adams,³⁹ J. K. Adkins,³⁰ G. Agakishiev,²⁸ I. Aggarwal,⁴¹ M. M. Aggarwal,⁴¹ Z. Ahammed,⁶¹ I. Alekseev,^{3,35} D. M. Anderson,⁵⁵ A. Aparin,²⁸ E. C. Aschenauer,⁶ M. U. Ashraf,¹¹ F. G. Atetalla,²⁹ A. Attri,⁴¹ G. S. Averichev,²⁸ V. Bairathi,⁵³ W. Baker,¹⁰ J. G. Ball Cap,²⁰ K. Barish,¹⁰ A. Behera,⁵² R. Bellwied,²⁰ P. Bhagat,²⁷ A. Bhasin,²⁷ J. Bielcik,¹⁴ J. Bielcikova,³⁸ I. G. Bordyuzhin,³ J. D. Brandenburg,⁶ A. V. Brandin,³⁵ I. Bunzarov,²⁸ X. Z. Cai,⁵⁰ H. Caines,⁶⁴ M. Calderón de la Barca Sánchez,⁸ D. Cebra,⁸ I. Chakaberia,^{31,6} P. Chaloupka,¹⁴ B. K. Chan,⁹ F.-H. Chang,³⁷ Z. Chang,⁶ N. Chankova-Bunzarova,²⁸ A. Chatterjee,¹¹ S. Chattopadhyay,⁶¹ D. Chen,¹⁰ J. Chen,⁴⁹ J. H. Chen,¹⁸ X. Chen,⁴⁸ Z. Chen,⁴⁹ J. Cheng,⁵⁷ M. Chevalier,¹⁰ S. Choudhury,¹⁸ W. Christie,⁶ X. Chu,⁶ H. J. Crawford,⁷ M. Csanád,¹⁶ M. Daugherty,¹ T. G. Dedovich,²⁸ I. M. Deppner,¹⁹ A. A. Derevschikov,⁴³ A. Dhamija,⁴¹ L. Di Carlo,⁶³ L. Didenko,⁶ P. Dixit,²² X. Dong,³¹ J. L. Drachenberg,¹ E. Duckworth,²⁹ J. C. Dunlop,⁶ N. Elsey,⁶³ J. Engelage,⁷ G. Eppley,⁴⁵ S. Esumi,⁵⁸ O. Evdokimov,¹² A. Ewigleben,³² O. Eyser,⁶ R. Fatemi,³⁰ F. M. Fawzi,⁵ S. Fazio,⁶ P. Federic,³⁸ J. Fedorisin,²⁸ C. J. Feng,³⁷ Y. Feng,⁴⁴ P. Filip,²⁸ E. Finch,⁵¹ Y. Fisyak,⁶ A. Francisco,⁶⁴ C. Fu,¹¹ L. Fulek,² C. A. Gagliardi,⁵⁵ T. Galatyuk,¹⁵ F. Geurts,⁴⁵ N. Ghimire,⁵⁴ A. Gibson,⁶⁰ K. Gopal,²³ X. Gou,⁴⁹ D. Grosnick,⁶⁰ A. Gupta,²⁷ W. Guryn,⁶ A. I. Hamad,²⁹ A. Hamed,⁵ Y. Han,⁴⁵ S. Harabasz,¹⁵ M. D. Harasty,⁸ J. W. Harris,⁶⁴ H. Harrison,³⁰ S. He,¹¹ W. He,¹⁸ X. H. He,²⁶ Y. He,⁴⁹ S. Heppelmann,⁸ S. Heppelmann,⁴² N. Herrmann,¹⁹ E. Hoffman,²⁰ L. Holub,¹⁴ Y. Hu,¹⁸ H. Huang,³⁷ H. Z. Huang,⁹ S. L. Huang,⁵² T. Huang,³⁷ X. Huang,⁵⁷ Y. Huang,⁵⁷ T. J. Humanic,³⁹ G. Igo,^{9,*} D. Isenhower,¹ W. W. Jacobs,²⁵ C. Jena,²³ A. Jentsch,⁶ Y. Ji,³¹ J. Jia,^{6,52} K. Jiang,⁴⁸ X. Ju,⁴⁸ E. G. Judd,⁷ S. Kabana,⁵³ M. L. Kabir,¹⁰ S. Kagamaster,³² D. Kalinkin,^{25,6} K. Kang,⁵⁷ D. Kapukchyan,¹⁰ K. Kauder,⁶ H. W. Ke,⁶ D. Keane,²⁹ A. Kechechyan,²⁸ M. Kelsey,⁶³ Y. V. Khyzhniak,³⁵ D. P. Kikola,⁶² C. Kim,¹⁰ B. Kimelman,⁸ D. Kincses,¹⁶ I. Kisel,¹⁷ A. Kiselev,⁶ A. G. Knospe,³² H. S. Ko,³¹ L. Kochenda,³⁵ L. K. Kosarzewski,¹⁴ L. Kramerik,¹⁴ P. Kravtsov,³⁵ L. Kumar,⁴¹ S. Kumar,²⁶ R. Kunnawalkam Elayavalli,⁶⁴ J. H. Kwasizur,²⁵ R. Lacey,⁵² S. Lan,¹¹ J. M. Landgraf,⁶ J. Lauret,⁶ A. Lebedev,⁶ R. Lednicky,^{28,38} J. H. Lee,⁶ Y. H. Leung,³¹ N. Lewis,⁶ C. Li,⁴⁹ C. Li,⁴⁸ W. Li,⁴⁵ X. Li,⁴⁸ Y. Li,⁵⁷ X. Liang,¹⁰ Y. Liang,²⁹ R. Licenik,³⁸ T. Lin,⁴⁹ Y. Lin,¹¹ M. A. Lisa,³⁹ F. Liu,¹¹ H. Liu,²⁵ H. Liu,¹¹ P. Liu,⁵² T. Liu,⁶⁴ X. Liu,³⁹ Y. Liu,⁵⁵ Z. Liu,⁴⁸ T. Ljubicic,⁶ W. J. Llope,⁶³ R. S. Longacre,⁶ E. Loyd,¹⁰ N. S. Lukow,⁵⁴ X. F. Luo,¹¹ L. Ma,¹⁸ R. Ma,⁶ Y. G. Ma,¹⁸ N. Magdy,¹² D. Mallick,³⁶ S. Margetis,²⁹ C. Markert,⁵⁶ H. S. Matis,³¹ J. A. Mazer,⁴⁶ N. G. Minaev,⁴³ S. Mioduszewski,⁵⁵ B. Mohanty,³⁶ M. M. Mondal,⁵² I. Mooney,⁶³ D. A. Morozov,⁴³ A. Mukherjee,¹⁶ M. Nagy,¹⁶ J. D. Nam,⁵⁴ Md. Nasim,²² K. Nayak,¹¹ D. Neff,⁹ J. M. Nelson,⁷ D. B. Nemes,⁶⁴ M. Nie,⁴⁹ G. Nigmatkulov,³⁵ T. Niida,⁵⁸ R. Nishitani,⁵⁸ L. V. Nogach,⁴³ T. Nonaka,⁵⁸ A. S. Nunes,⁶ G. Odyniec,³¹ A. Ogawa,⁶ S. Oh,³¹ V. A. Okorokov,³⁵ B. S. Page,⁶ R. Pak,⁶ J. Pan,⁵⁵ A. Pandav,³⁶ A. K. Pandey,⁵⁸ Y. Panebratsev,²⁸ P. Parfenov,³⁵ B. Pawlik,⁴⁰ D. Pawlowska,⁶² C. Perkins,⁷ L. Pinsky,²⁰ R. L. Pintér,¹⁶ J. Pluta,⁶² B. R. Pokhrel,⁵⁴ G. Ponimatkin,³⁸ J. Porter,³¹ M. Posik,⁵⁴ V. Prozorova,¹⁴ N. K. Pruthi,⁴¹ M. Przybycien,² J. Putschke,⁶³ H. Qiu,²⁶ A. Quintero,⁵⁴ C. Racz,¹⁰ S. K. Radhakrishnan,²⁹ N. Raha,⁶³ R. L. Ray,⁵⁶ R. Reed,³² H. G. Ritter,³¹ M. Robotkova,³⁸ O. V. Rogachevskiy,²⁸ J. L. Romero,⁸ D. Roy,⁴⁶ L. Ruan,⁶ J. Rusnak,³⁸ A. K. Sahoo,²² N. R. Sahoo,⁴⁹ H. Sako,⁵⁸ S. Salur,⁴⁶ J. Sandweiss,^{64,*} S. Sato,⁵⁸ W. B. Schmidke,⁶ N. Schmitz,³³ B. R. Schweid,⁵² F. Seck,¹⁵ J. Seger,¹³ M. Sergeeva,⁹ R. Seto,¹⁰ P. Seyboth,³³ N. Shah,²⁴ E. Shahaliev,²⁸ P. V. Shanmuganathan,⁶ M. Shao,⁴⁸ T. Shao,¹⁸ A. I. Sheikh,²⁹ D. Y. Shen,¹⁸ S. S. Shi,¹¹ Y. Shi,⁴⁹ Q. Y. Shou,¹⁸ E. P. Sichtermann,³¹ R. Sikora,² M. Simko,³⁸ J. Singh,⁴¹ S. Singha,²⁶ M. J. Skoby,⁴⁴ N. Smirnov,⁶⁴ Y. Söhnngen,¹⁹ W. Solyst,²⁵ P. Sorensen,⁶ H. M. Spinka,^{4,*} B. Srivastava,⁴⁴ T. D. S. Stanislaus,⁶⁰ M. Stefaniak,⁶² D. J. Stewart,⁶⁴ M. Strikhanov,³⁵ B. Stringfellow,⁴⁴ A. A. P. Suaide,⁴⁷ M. Sumner,³⁸ B. Summa,⁴² X. M. Sun,¹¹ X. Sun,¹² Y. Sun,⁴⁸ Y. Sun,²¹ B. Surrow,⁵⁴ D. N. Svirida,³ Z. W. Sweger,⁸ P. Szymanski,⁶² A. H. Tang,⁶ Z. Tang,⁴⁸ A. Taranenko,³⁵ T. Tarnowsky,³⁴ J. H. Thomas,³¹ A. R. Timmins,²⁰ D. Tlusty,¹³ T. Todoroki,⁵⁸ M. Tokarev,²⁸ C. A. Tomkiel,³² S. Trentalange,⁹ R. E. Tribble,⁵⁵ P. Tribedy,⁶ S. K. Tripathy,¹⁶ T. Truhlar,¹⁴ B. A. Trzeciak,¹⁴ O. D. Tsai,⁹ Z. Tu,⁶ T. Ullrich,⁶ D. G. Underwood,^{4,60} I. Upsal,⁴⁵ G. Van Buren,⁶ J. Vanek,³⁸ A. N. Vasiliev,⁴³ I. Vassiliev,¹⁷ V. Verkest,⁶³ F. Videbæk,⁶ S. Vokal,²⁸ S. A. Voloshin,⁶³ F. Wang,⁴⁴ G. Wang,⁹ J. S. Wang,²¹ P. Wang,⁴⁸ X. Wang,⁴⁹ Y. Wang,¹¹ Y. Wang,⁵⁷ Z. Wang,⁴⁹ J. C. Webb,⁶ P. C. Weidenkaff,¹⁹ L. Wen,⁹ G. D. Westfall,³⁴ H. Wieman,³¹ S. W. Wissink,²⁵ R. Witt,⁵⁹ J. Wu,¹¹ J. Wu,²⁶ Y. Wu,¹⁰ B. Xi,⁵⁰ Z. G. Xiao,⁵⁷ G. Xie,³¹ W. Xie,⁴⁴ H. Xu,²¹ N. Xu,³¹ Q. H. Xu,⁴⁹ Y. Xu,⁴⁹ Z. Xu,⁶ Z. Xu,⁹ G. Yan,⁴⁹ C. Yang,⁴⁹

Q. Yang,⁴⁹ S. Yang,⁴⁵ Y. Yang,³⁷ Z. Ye,⁴⁵ Z. Ye,¹² L. Yi,⁴⁹ K. Yip,⁶ Y. Yu,⁴⁹ H. Zbroszczyk,⁶² W. Zha,⁴⁸
 C. Zhang,⁵² D. Zhang,¹¹ J. Zhang,⁴⁹ S. Zhang,¹² S. Zhang,¹⁸ X. P. Zhang,⁵⁷ Y. Zhang,²⁶ Y. Zhang,⁴⁸ Y. Zhang,¹¹
 Z. J. Zhang,³⁷ Z. Zhang,⁶ Z. Zhang,¹² J. Zhao,⁴⁴ C. Zhou,¹⁸ Y. Zhou,¹¹ X. Zhu,⁵⁷ M. Zurek,⁴ and M. Zyzak¹⁷

(STAR Collaboration)

- ¹Abilene Christian University, Abilene, Texas 79699
²AGH University of Science and Technology, FPACS, Cracow 30-059, Poland
³Alikhanov Institute for Theoretical and Experimental Physics NRC "Kurchatov Institute", Moscow 117218, Russia
⁴Argonne National Laboratory, Argonne, Illinois 60439
⁵American University of Cairo, New Cairo 11835, New Cairo, Egypt
⁶Brookhaven National Laboratory, Upton, New York 11973
⁷University of California, Berkeley, California 94720
⁸University of California, Davis, California 95616
⁹University of California, Los Angeles, California 90095
¹⁰University of California, Riverside, California 92521
¹¹Central China Normal University, Wuhan, Hubei 430079
¹²University of Illinois at Chicago, Chicago, Illinois 60607
¹³Creighton University, Omaha, Nebraska 68178
¹⁴Czech Technical University in Prague, FNSPE, Prague 115 19, Czech Republic
¹⁵Technische Universität Darmstadt, Darmstadt 64289, Germany
¹⁶ELTE Eötvös Loránd University, Budapest, Hungary H-1117
¹⁷Frankfurt Institute for Advanced Studies FIAS, Frankfurt 60438, Germany
¹⁸Fudan University, Shanghai, 200433
¹⁹University of Heidelberg, Heidelberg 69120, Germany
²⁰University of Houston, Houston, Texas 77204
²¹Huzhou University, Huzhou, Zhejiang 313000
²²Indian Institute of Science Education and Research (IISER), Berhampur 760010, India
²³Indian Institute of Science Education and Research (IISER) Tirupati, Tirupati 517507, India
²⁴Indian Institute Technology, Patna, Bihar 801106, India
²⁵Indiana University, Bloomington, Indiana 47408
²⁶Institute of Modern Physics, Chinese Academy of Sciences, Lanzhou, Gansu 730000
²⁷University of Jammu, Jammu 180001, India
²⁸Joint Institute for Nuclear Research, Dubna 141 980, Russia
²⁹Kent State University, Kent, Ohio 44242
³⁰University of Kentucky, Lexington, Kentucky 40506-0055
³¹Lawrence Berkeley National Laboratory, Berkeley, California 94720
³²Lehigh University, Bethlehem, Pennsylvania 18015
³³Max-Planck-Institut für Physik, Munich 80805, Germany
³⁴Michigan State University, East Lansing, Michigan 48824
³⁵National Research Nuclear University MEPHI, Moscow 115409, Russia
³⁶National Institute of Science Education and Research, HBNI, Jatni 752050, India
³⁷National Cheng Kung University, Tainan 70101
³⁸Nuclear Physics Institute of the CAS, Rez 250 68, Czech Republic
³⁹Ohio State University, Columbus, Ohio 43210
⁴⁰Institute of Nuclear Physics PAN, Cracow 31-342, Poland
⁴¹Panjab University, Chandigarh 160014, India
⁴²Pennsylvania State University, University Park, Pennsylvania 16802
⁴³NRC "Kurchatov Institute", Institute of High Energy Physics, Protvino 142281, Russia
⁴⁴Purdue University, West Lafayette, Indiana 47907
⁴⁵Rice University, Houston, Texas 77251
⁴⁶Rutgers University, Piscataway, New Jersey 08854
⁴⁷Universidade de São Paulo, São Paulo, Brazil 05314-970
⁴⁸University of Science and Technology of China, Hefei, Anhui 230026
⁴⁹Shandong University, Qingdao, Shandong 266237
⁵⁰Shanghai Institute of Applied Physics, Chinese Academy of Sciences, Shanghai 201800
⁵¹Southern Connecticut State University, New Haven, Connecticut 06515
⁵²State University of New York, Stony Brook, New York 11794
⁵³Instituto de Alta Investigación, Universidad de Tarapacá, Arica 1000000, Chile
⁵⁴Temple University, Philadelphia, Pennsylvania 19122
⁵⁵Texas A&M University, College Station, Texas 77843
⁵⁶University of Texas, Austin, Texas 78712
⁵⁷Tsinghua University, Beijing 100084
⁵⁸University of Tsukuba, Tsukuba, Ibaraki 305-8571, Japan

⁵⁹United States Naval Academy, Annapolis, Maryland 21402

⁶⁰Valparaiso University, Valparaiso, Indiana 46383

⁶¹Variable Energy Cyclotron Centre, Kolkata 700064, India

⁶²Warsaw University of Technology, Warsaw 00-661, Poland

⁶³Wayne State University, Detroit, Michigan 48201

⁶⁴Yale University, New Haven, Connecticut 06520

We report precision measurements of hypernuclei ${}^3_{\Lambda}\text{H}$ and ${}^4_{\Lambda}\text{H}$ lifetimes obtained from Au+Au collisions at $\sqrt{s_{\text{NN}}} = 3.0$ GeV and 7.2 GeV collected by the STAR experiment at RHIC, and the first measurement of ${}^3_{\Lambda}\text{H}$ and ${}^4_{\Lambda}\text{H}$ mid-rapidity yields in Au+Au collisions at $\sqrt{s_{\text{NN}}} = 3.0$ GeV. The lifetimes are measured to be $221 \pm 15(\text{stat.}) \pm 19(\text{syst.})$ ps for ${}^3_{\Lambda}\text{H}$ and $218 \pm 6(\text{stat.}) \pm 13(\text{syst.})$ ps for ${}^4_{\Lambda}\text{H}$. The p_T -integrated yields of ${}^3_{\Lambda}\text{H}$ and ${}^4_{\Lambda}\text{H}$ are presented in different centrality and rapidity intervals. It is observed that the shape of the rapidity distribution of ${}^4_{\Lambda}\text{H}$ is different for 0–10% and 10–50% centrality collisions. Thermal model calculations, using the canonical ensemble for strangeness, describes the ${}^3_{\Lambda}\text{H}$ yield well, while underestimating the ${}^4_{\Lambda}\text{H}$ yield. Transport models, combining baryonic mean-field and coalescence (JAM) or utilizing dynamical cluster formation via baryonic interactions (PHQMD) for light nuclei and hypernuclei production, approximately describe the measured ${}^3_{\Lambda}\text{H}$ and ${}^4_{\Lambda}\text{H}$ yields.

Hypernuclei are nuclei containing at least one hyperon. As such, they are excellent experimental probes to study the hyperon-nucleon ($Y-N$) interaction. The $Y-N$ interaction is an important ingredient, not only in the equation-of-state (EoS) of astrophysical objects such as neutron stars, but also in the description of the hadronic phase of a heavy-ion collision [1]. Heavy-ion collisions provide a unique laboratory to investigate the $Y-N$ interaction in finite temperature and density regions through the measurements of hypernuclei lifetimes, production yields etc.

The lifetimes of hypernuclei ranging from $A = 3$ to 56 have previously been reported [2–11]. The mesonic decay width dominates for $A \leq 5$ hypernuclei, and variations in the lifetimes of light systems have been observed [3–6], likely due to the sensitivity of the mesonic decay width to hypernuclear shell structure [12]. In particular, the hypertriton ${}^3_{\Lambda}\text{H}$, a bound state of Λpn , has a very small Λ separation energy of several hundred keV [13, 14], suggesting that the ${}^3_{\Lambda}\text{H}$ lifetime is close to the free- Λ lifetime. Recently, STAR [10, 11], ALICE [7, 8] and HypHI [9] have reported ${}^3_{\Lambda}\text{H}$ lifetimes ranging from $\sim 50\%$ to $\sim 100\%$ of the free- Λ lifetime. The tension between the measurements has led to debate [15]. This calls for more precise measurements of the ${}^3_{\Lambda}\text{H}$ lifetime to resolve the puzzle.

In heavy-ion collisions, light hypernuclei are expected to be abundantly produced at low energies due to the high baryon density [1, 16], while hypernuclear production mechanisms are not well understood. Coalescence of hyperons and nucleons has been proposed as a possible production mechanism, particularly in central heavy-ion collisions [17], while in peripheral collisions production via the absorption of hyperons in the spectator fragments has been suggested [18]. In statistical thermal models, effects from canonical suppression for strangeness are expected to come into play at low energies. These effects are not well constrained, introducing additional challenges for thermal model predictions [19].

At high collision energies, the ${}^3_{\Lambda}\text{H}$ yields have been measured by ALICE [8] and STAR [10]. ALICE results from Pb+Pb collisions at 2.76 TeV are consistent with thermal model predictions [16] and UrQMD [1]. Meanwhile, significant differences are seen for these two theoretical calculations at low energies. The HypHI Collaboration has measured the hypernuclei cross sections at $\sqrt{s_{\text{NN}}} = 2.7$ GeV in ${}^6\text{Li} + {}^{12}\text{C}$ collisions [20], however the measurement suffered from low statistics and lack of mid-rapidity coverage. The production mechanisms of hypernuclei at lower energies remain an open question. Also, the measurements of the production yields of hypernuclei are critical for understanding the role of hyperons and strangeness in the EoS in the high-baryon-density region [21].

In this letter, we report ${}^3_{\Lambda}\text{H}$ and ${}^4_{\Lambda}\text{H}$ lifetimes obtained from data samples of Au+Au collisions at $\sqrt{s_{\text{NN}}} = 3.0$ GeV and 7.2 GeV, as well as the first measurement of ${}^3_{\Lambda}\text{H}$ and ${}^4_{\Lambda}\text{H}$ differential yields at $\sqrt{s_{\text{NN}}} = 3.0$ GeV. We focus on the yields at mid-rapidity in order to investigate hypernuclear production in the high-baryon-density region. The yields at $\sqrt{s_{\text{NN}}} = 7.2$ GeV are not presented here due to the lack of mid-rapidity coverage. The data were collected by the Solenoidal Tracker at RHIC (STAR) in 2018, using the fixed-target (FXT) configuration. In the FXT configuration a single beam provided by RHIC impinges on a gold target of thickness 0.25 mm (corresponding to a 1% interaction probability) located at 201 cm away from the center of the STAR detector. The minimum bias (MB) trigger condition is provided by the Beam-Beam Counters (BBC) [22] and the Time of Flight (TOF) detector [23]. The reconstructed primary-vertex position along the beam direction is required to be within ± 2 cm of the nominal target position. The primary-vertex position in the radial plane is required to lie within a radius of 1.5 cm from the center of the target to eliminate possible backgrounds arising from interactions with the vacuum pipe. In total, 2.8×10^8 (1.5×10^8) qualified events at $\sqrt{s_{\text{NN}}} = 3.0$ (7.2) GeV are used in

this analysis. The $\sqrt{s_{NN}} = 3.0$ GeV analysis and $\sqrt{s_{NN}} = 7.2$ GeV analysis are similar. In the following, we describe the $\sqrt{s_{NN}} = 3.0$ GeV analysis; details related to the $\sqrt{s_{NN}} = 7.2$ GeV analysis can be found in the supplementary material.

The centrality of the collision is determined using the number of reconstructed charged tracks in the Time Projection Chamber (TPC) [24] compared to a Monte Carlo Glauber model simulation [25]. The top 0–50% most central events are selected for our analysis. ${}^3_{\Lambda}\text{H}$ and ${}^4_{\Lambda}\text{H}$ are reconstructed via the two-body decay channels ${}^A_{\Lambda}\text{H} \rightarrow \pi^- + {}^A\text{He}$, where $A = 3, 4$. Charged tracks are reconstructed using the TPC in a 0.5 Tesla uniform magnetic field. We require the reconstructed tracks to have at least 15 measured space points in the TPC (out of 45) and a minimum reconstructed transverse momentum of 150 MeV/c to ensure good track quality. Particle identification for π^- , ${}^3\text{He}$, and ${}^4\text{He}$ is achieved by the measured ionization energy loss in the TPC. The KFPARTICLE package [26], a particle reconstruction package based on the Kalman filter utilizing the error matrices, is used for the reconstruction of the mother particle. Various topological variables such as the decay length of the mother particle, the distances of closest approach (DCA) between the mother/daughter particles to the primary vertex, and the DCA between the two daughters, are examined. Cuts on these topological variables are applied to the hypernuclei candidates in order to optimize the signal significance. In addition, we place fiducial cuts on the reconstructed particles to minimize edge effects.

Figure 1 (a,b) shows invariant mass distributions of ${}^3\text{He}\pi^-$ pairs and ${}^4\text{He}\pi^-$ pairs in the p_T region (1.0–4.0) GeV/c for the 50% most central collisions. The combinatorial background is estimated using a rotational technique, in which all π^- tracks in a single event are rotated with a fixed angle multiple times and then normalized in the side-band region. The background shape is reasonably reproduced using this rotation technique for both ${}^3_{\Lambda}\text{H}$ and ${}^4_{\Lambda}\text{H}$ as shown in Fig. 1. The combinatorial background is subtracted from the data in 2D phase space (p_T and rapidity y) in the collision center-of-mass frame. In addition to subtracting the rotational background, we perform a linear fit using the side-band region to remove any residual background. The subtracted distributions are shown in Fig. 1 (c,d). The target is located at $y = -1.05$, and the sign of the rapidity y is chosen such that the beam travels in the positive y direction. The mass resolution is 1.5 and 1.8 MeV/ c^2 for ${}^3_{\Lambda}\text{H}$ and ${}^4_{\Lambda}\text{H}$, respectively.

The reconstructed ${}^3_{\Lambda}\text{H}$ and ${}^4_{\Lambda}\text{H}$ candidates are further divided into different $L/\beta\gamma$ intervals, where L is the decay length, β and γ are particle velocity divided by the speed of light and Lorentz factor, respectively. The raw signal counts, N^{raw} , for each $L/\beta\gamma$ interval are corrected for the detector acceptance and reconstruction efficiency ($\varepsilon_{\text{TPC}} \times \varepsilon_{\text{PID}}$) using an embedding technique in which

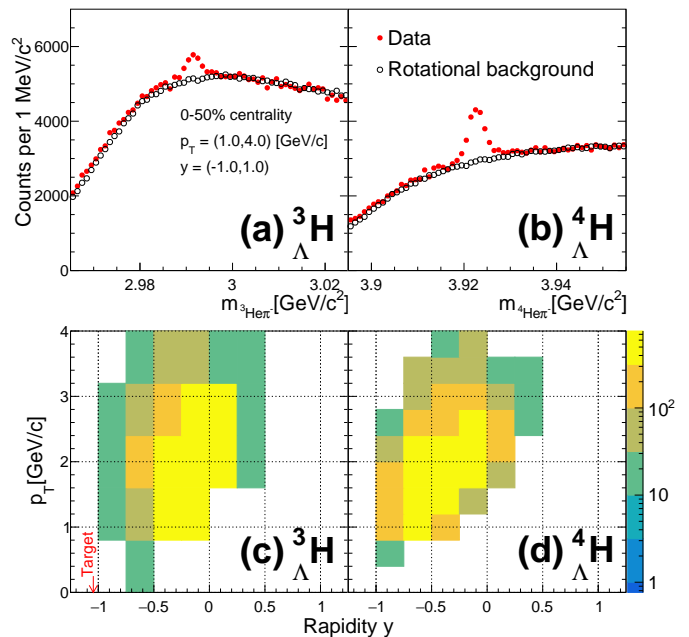


FIG. 1: Top row: Invariant mass distributions of (a) ${}^3\text{He}\pi^-$ and (b) ${}^4\text{He}\pi^-$ pairs reconstructed from data are shown by solid red circles. Open black circles represent the background constructed by using rotated pion tracks. Bottom row: The transverse momentum (p_T) versus the rapidity (y) for reconstructed (c) ${}^3_{\Lambda}\text{H}$ and (d) ${}^4_{\Lambda}\text{H}$. The target is located at the $y = -1.05$.

the TPC response to Monte Carlo (MC) hypernuclei and their decay daughters is simulated in the STAR detector described in GEANT3 [27]. Simulated signals are embedded into the real data and processed through the same reconstruction algorithm as in real data. The simulated hypernuclei, used for determining the efficiency correction, need to be re-weighted in 2D phase space (p_T – y) such that the MC hypernuclei are distributed in a realistic manner. This can be constrained by comparing the reconstructed kinematic distributions between simulation and real data. The corrected hypernuclei yield as a function of $L/\beta\gamma$ is fitted with an exponential function (see supplementary material) and the decay lifetime is determined as the negative inverse of the slope divided by the speed of light.

We consider four major sources of systematic uncertainties in the lifetime result: imperfect description of topological variables in the simulations, imperfect knowledge of the true kinematic distribution of the hypernuclei, the TPC tracking efficiency, and the signal extraction technique. Their contributions are estimated by varying the topological cuts, the MC hypernuclei p_T – y distributions, the TPC track quality selection cuts and the background subtraction method. The possible contamination of the signal due to multi-body decays of $A > 3$ hypernuclei is estimated using MC simulations and found to be negligible ($< 0.1\%$) within our reconstructed hyper-

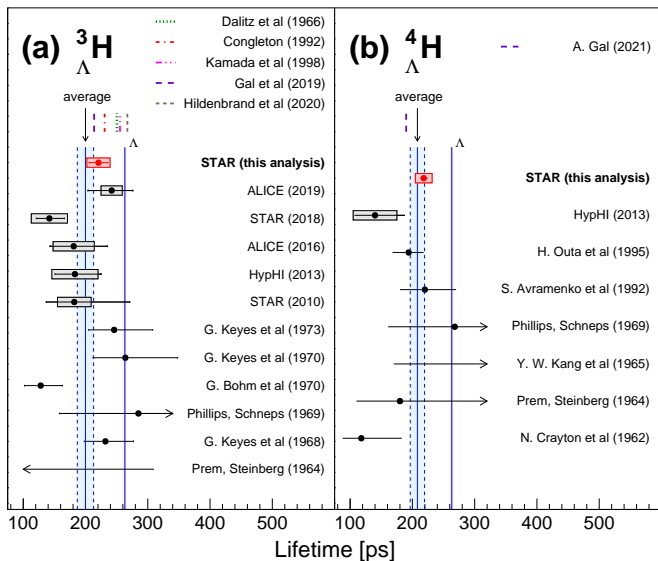


FIG. 2: ${}^3_{\Lambda}\text{H}$ (a) and ${}^4_{\Lambda}\text{H}$ (b) measured lifetime, compared to previous measurements [3–5, 7–11, 28–34], theoretical calculations [35–40] and the free- Λ lifetime [41]. Horizontal lines represent statistical uncertainties, while boxes represent systematic uncertainties. The experimental average lifetimes and the corresponding uncertainty of ${}^3_{\Lambda}\text{H}$ and ${}^4_{\Lambda}\text{H}$ are also shown as vertical blue shaded bands.

nuclei mass window. The systematic uncertainties due to different sources are tabulated in Tab. I. They are assumed to be uncorrelated with each other and added in quadrature in the total systematic uncertainty. As a cross-check, we conducted the measurement of Λ lifetime from the same data and the result is consistent with the PDG value [41] (see supplementary material).

Source	Lifetime		dN/dy	
	${}^3_{\Lambda}\text{H}$	${}^4_{\Lambda}\text{H}$	${}^3_{\Lambda}\text{H}$	${}^4_{\Lambda}\text{H}$
Analysis cuts	5.5%	5.1%	15.1%	6.9%
Input MC	3.1%	1.8%	8.8%	3.8%
Tracking efficiency	5.0%	2.4%	14.1%	5.2%
Signal extraction	1.5%	0.7%	14.3%	7.7%
Extrapolation	N/A	N/A	13.6%	10.9%
Detector material	< 1%	< 1%	4.0%	2.0%
Total	8.2%	6.0%	31.9%	16.6%

TABLE I: Summary of systematic uncertainties for the lifetime and top 10% most central dN/dy ($|y| < 0.5$) measurements using $\sqrt{s_{\text{NN}}} = 3.0$ GeV data.

The lifetime results measured at $\sqrt{s_{\text{NN}}} = 3.0$ GeV and $\sqrt{s_{\text{NN}}} = 7.2$ GeV are found to agree well with each other. The combined results are $221 \pm 15(\text{stat.}) \pm 19(\text{syst.})$ ps for ${}^3_{\Lambda}\text{H}$ and $218 \pm 6(\text{stat.}) \pm 13(\text{syst.})$ ps for ${}^4_{\Lambda}\text{H}$. As shown in Fig. 2, they are consistent with previous measurements from ALICE [7, 8], STAR [10, 11], HypHI [9] and early experiments using imaging techniques [3–5, 10, 28–34]. Using all the available experimental data, the average

lifetimes of ${}^3_{\Lambda}\text{H}$ and ${}^4_{\Lambda}\text{H}$ are 200 ± 13 ps and 208 ± 12 ps, respectively. These precise data clearly indicate that the ${}^3_{\Lambda}\text{H}$ and ${}^4_{\Lambda}\text{H}$ lifetimes are considerably lower than the free- Λ lifetime. We conclude that the ${}^3_{\Lambda}\text{H}$ lifetime puzzle is resolved on the experimental side.

Early theoretical calculations of the ${}^3_{\Lambda}\text{H}$ lifetime typically give values within 15% of the free- Λ lifetime τ_{Λ} [36–38]. This can be explained by the loose binding of Λ in the ${}^3_{\Lambda}\text{H}$. A recent calculation [35] using a pionless effective field theory approach with Λd degrees of freedom gives a ${}^3_{\Lambda}\text{H}$ lifetime of $\approx 98\%$ τ_{Λ} . Meanwhile, it is shown in recent studies that incorporating attractive pion final state interactions, which has been previously disregarded, decreases the ${}^3_{\Lambda}\text{H}$ lifetime by $\sim 15\%$ [15, 39]. This leads to a prediction of the ${}^3_{\Lambda}\text{H}$ lifetime to be $(81 \pm 2)\%$ of τ_{Λ} , consistent with the world average.

As for ${}^4_{\Lambda}\text{H}$, a recent estimation [40] based on the isospin rule [42] agrees with the data within 1σ . The empirical isospin rule is based on the observation that $\Gamma(\Lambda \rightarrow n + \pi^0)/\Gamma(\Lambda \rightarrow p + \pi^-) \approx 0.5$, which leads to the prediction $\tau({}^4_{\Lambda}\text{H})/\tau({}^4_{\Lambda}\text{He}) = (74 \pm 4)\%$ [40]. Combining the average value reported here and the previous ${}^4_{\Lambda}\text{He}$ lifetime measurement [43, 44], the measured ratio $\tau({}^4_{\Lambda}\text{H})/\tau({}^4_{\Lambda}\text{He})$ is $(83 \pm 6)\%$, consistent with the expectation.

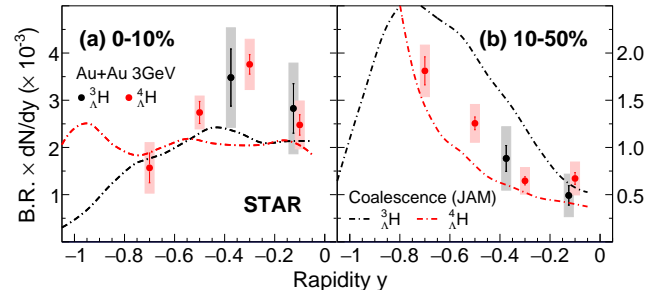


FIG. 3: B.R. $\times dN/dy$ as a function of rapidity y for ${}^3_{\Lambda}\text{H}$ (black circles) and ${}^4_{\Lambda}\text{H}$ (red circles) for (a) 0–10% centrality and (b) 10–50% centrality Au+Au collisions at $\sqrt{s_{\text{NN}}} = 3.0$ GeV. Vertical lines represent statistical uncertainties, while boxes represent systematic uncertainties. The dot-dashed lines represent coalescence (JAM) calculations. The coalescence parameters used are indicated in the text.

Heavy-ion collisions in the high-baryon-density region provide a unique opportunity for hypernuclear studies [16]. To further examine the hypernuclear structure and its production mechanism in heavy-ion collisions, we report the first measurement of hypernuclei dN/dy in two centrality selections: top 0–10% most central and 10–50% mid-central collisions. The p_T spectra can be found in the supplementary material, and are extrapolated down to zero p_T to obtain the p_T -integrated dN/dy . Different functions [45] are used to estimate the systematic uncertainties in the unmeasured region, which correspond to 32–60% of the p_T -integrated yield in various rapidity

intervals, and introduce 8–14% systematic uncertainties. Systematic uncertainties associated with analysis cuts, tracking efficiency, and signal extraction are estimated using the same method as for the lifetime measurement. We further consider the effect of the uncertainty in the simulated hypernuclei lifetime on the calculated reconstruction efficiency by varying the simulation's lifetime assumption within a 1σ window of the average experimental lifetime, which leads to 8% and 4% uncertainty for ${}^3_{\Lambda}\text{H}$ and ${}^4_{\Lambda}\text{H}$, respectively. Finally, hypernuclei may encounter Coulomb dissociation when traversing the gold target. The survival probability is estimated using a Monte Carlo method according to [46]. The results show the survival probability $> 96(99)\%$ for ${}^3_{\Lambda}\text{H}$ (${}^4_{\Lambda}\text{H}$) in the kinematic regions considered for the analysis. The dissociation has a strong dependence on the Λ -separation energy (B_{Λ}) of the hypernuclei. Systematic uncertainties are estimated by varying the B_{Λ} of the ${}^3_{\Lambda}\text{H}$ and ${}^4_{\Lambda}\text{H}$, which are equal to 0.27 ± 0.08 MeV and 2.53 ± 0.04 MeV, respectively [47]. As a conservative estimate, we assign the systematic uncertainty by comparing the calculation using the central values of B_{Λ} and its 2.5σ limits. A summary of the systematic uncertainties for the dN/dy measurement is listed in Tab. I.

The p_{T} -integrated yields of ${}^3_{\Lambda}\text{H}$ and ${}^4_{\Lambda}\text{H}$ times the branching ratio (B.R.) as a function of y are shown in Fig. 3. For ${}^4_{\Lambda}\text{H}$, we can see that the mid-rapidity distribution changes from convex to concave from 0–10% to 10–50% centrality. This change in shape is likely related to the change in the collision geometry, such as spectators playing a larger role in non-central collisions.

To interpret the data, calculations from the transport model, JET AA Microscopic Transportation Model (JAM) [48] are used to model the dynamical stage of the reaction. The coalescence prescription is subsequently applied to all produced hadrons as an afterburner [49]. In this model, deuterons and tritons are formed through the coalescence of nucleons, and subsequently, ${}^3_{\Lambda}\text{H}$ and ${}^4_{\Lambda}\text{H}$ are formed through the coalescence of Λ baryons with deuterons or tritons. Coalescence takes place if the relative momenta of the constituents are within a sphere of radius p_C and the spacial coordinates are within a sphere of radius r_C . It is found that calculations using coalescence parameters (r_C, p_C) of (4.5fm, 0.3GeV/c), (4fm, 0.3GeV/c), (4fm, 0.12GeV/c) and (4fm, 0.3GeV/c) for $d, t, {}^3_{\Lambda}\text{H}$ and ${}^4_{\Lambda}\text{H}$ respectively can qualitatively reproduce the centrality and rapidity dependence of the measured yields. The smaller p_C parameter used for ${}^3_{\Lambda}\text{H}$ formation is motivated by its much smaller B_{Λ} (~ 0.3 MeV) compared to ${}^4_{\Lambda}\text{H}$ (~ 2.6 MeV). A detailed study on the coalescence parameter dependence of the calculated yields is beyond the scope of this paper.

The decay B.R. of ${}^3_{\Lambda}\text{H} \rightarrow {}^3\text{He} + \pi^-$ was not directly measured. A variation in the range 15 – 35% for the B.R. [11, 37, 38] is considered when calculating the total

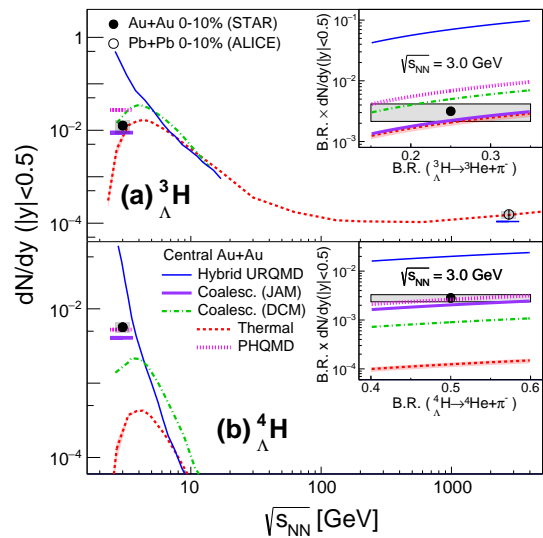


FIG. 4: (a) ${}^3_{\Lambda}\text{H}$ and (b) ${}^4_{\Lambda}\text{H}$ yields at $|y| < 0.5$ as a function of beam energy in central heavy-ion collisions. The symbols represent measurements [8] while the lines represent different theoretical calculations. The data points assume a B.R. of 25(50)% for ${}^3_{\Lambda}\text{H}({}^4_{\Lambda}\text{H}) \rightarrow {}^3\text{He}({}^4\text{He}) + \pi^-$. The insets show the (a) ${}^3_{\Lambda}\text{H}$ and (b) ${}^4_{\Lambda}\text{H}$ yields at $|y| < 0.5$ times the B.R. as a function of the B.R.. Vertical lines represent statistical uncertainties, while boxes represent systematic uncertainties.

dN/dy . For ${}^4_{\Lambda}\text{H} \rightarrow {}^4\text{He} + \pi^-$, a variation of 40 – 60% based on [13, 43] is considered in this analysis.

The ${}^3_{\Lambda}\text{H}$ and ${}^4_{\Lambda}\text{H}$ mid-rapidity yields for central collisions as a function of center-of-mass energy are shown in Fig. 4, and are compared to theoretical models. The uncertainties on the B.R.s are not shown in the main panels. Instead, the insets show the $dN/dy \times \text{B.R.}$ as a function of B.R..

Several theoretical models are compared to our data, shown in Fig. 4. The thermal model adopts the canonical ensemble for strangeness [50] and can describe the mid-rapidity ${}^3_{\Lambda}\text{H}$ yield data at 3.0 GeV and 2.76 TeV. Canonical ensemble thermal statistics is mandatory to account for the large ϕ/K^- and ϕ/Ξ^- ratios measured at 3.0 GeV [25]. The UrQMD-hydro hybrid model however, overestimates our measurements by an order of magnitude. Coalescence calculations using DCM, an intranuclear cascade model to describe the dynamical stage of the reaction [1], are consistent with the ${}^3_{\Lambda}\text{H}$ yield while underestimating the ${}^4_{\Lambda}\text{H}$ yield, whereas the coalescence (JAM) calculations are consistent with both ${}^3_{\Lambda}\text{H}$ and ${}^4_{\Lambda}\text{H}$ yields. We note that in the DCM model, the same coalescence parameters are assumed for ${}^3_{\Lambda}\text{H}$ and ${}^4_{\Lambda}\text{H}$, while in the JAM model, parameters are tuned separately for ${}^3_{\Lambda}\text{H}$ and ${}^4_{\Lambda}\text{H}$ to fit the data. It is expected that the calculated hypernuclei yields depend on the choice of the coalescence parameters [1], and our measurement provides a new baseline for such parameters in coalescence models. Recent calculations from PHQMD [51, 52], a

microscopic transport model which utilizes a dynamical description of hypernuclei formation, is consistent with the measured yields within uncertainties. Compared to the JAM model which adopts a baryonic mean-field approach, baryonic interactions in PHQMD are modelled by density dependent 2-body baryonic potentials. These 2-body interactions are responsible for the dynamical formation of hypernuclei from hyperons and baryons in PHQMD. Since ${}^3_{\Lambda}\text{H}$ and ${}^4_{\Lambda}\text{H}$ are fragile objects, they are most likely formed at later times of the collision where the density is low enough that the objects formed are not immediately destroyed. Thus, our measurements not only provide quantitative input on the production mechanisms of loosely bound objects in heavy-ion collisions, but may also give information on the time evolution of the high baryon density medium formed.

In summary, precise measurements of ${}^3_{\Lambda}\text{H}$ and ${}^4_{\Lambda}\text{H}$ lifetimes have been obtained using the data samples of Au+Au collisions at 3.0 and 7.2 GeV. The lifetimes are measured to be $221 \pm 15(\text{stat.}) \pm 19(\text{syst.})$ ps for ${}^3_{\Lambda}\text{H}$ and $218 \pm 6(\text{stat.}) \pm 13(\text{syst.})$ ps for ${}^4_{\Lambda}\text{H}$. The averaged ${}^3_{\Lambda}\text{H}$ and ${}^4_{\Lambda}\text{H}$ lifetimes combining all existing measurements are both considerably smaller than the free- Λ lifetime. The precise ${}^3_{\Lambda}\text{H}$ lifetime reported here brings closure to the ${}^3_{\Lambda}\text{H}$ lifetime puzzle on the experimental side. We also present the first measurement of rapidity density of ${}^3_{\Lambda}\text{H}$ and ${}^4_{\Lambda}\text{H}$ in 0–10% and 10–50% 3.0 GeV Au+Au collisions. Thermal model with canonical ensemble for strangeness reproduces the mid-rapidity ${}^3_{\Lambda}\text{H}$ yield, but underestimates the ${}^4_{\Lambda}\text{H}$ yield. Hadronic transport models JAM and PHQMD calculations reproduce the measured midrapidity ${}^3_{\Lambda}\text{H}$ and ${}^4_{\Lambda}\text{H}$ yields reasonably well. New data from the Beam Energy Scan II program ($3 < \sqrt{s_{\text{NN}}} < 20$ GeV) offer extensive hypernuclei measurements to provide enhanced model discrimination power, giving insight on the production mechanisms of light hypernuclei and the Y - N interaction in the high-baryon-density region.

We thank the RHIC Operations Group and RCF at BNL, the NERSC Center at LBNL, and the Open Science Grid consortium for providing resources and support. This work was supported in part by the Office of Nuclear Physics within the U.S. DOE Office of Science, the U.S. National Science Foundation, the Ministry of Education and Science of the Russian Federation, National Natural Science Foundation of China, Chinese Academy of Science, the Ministry of Science and Technology of China and the Chinese Ministry of Education, the Higher Education Sprout Project by Ministry of Education at NCKU, the National Research Foundation of Korea, Czech Science Foundation and Ministry of Education, Youth and Sports of the Czech Republic, Hungarian National Research, Development and Innovation Office, New National Excellency Programme of the Hungarian Ministry of Human Capacities, Department of Atomic Energy and Department of Science and Tech-

nology of the Government of India, the National Science Centre of Poland, the Ministry of Science, Education and Sports of the Republic of Croatia, RosAtom of Russia and German Bundesministerium für Bildung, Wissenschaft, Forschung und Technologie (BMBF), Helmholtz Association, Ministry of Education, Culture, Sports, Science, and Technology (MEXT) and Japan Society for the Promotion of Science (JSPS).

* Deceased

- [1] J. Steinheimer et al., Phys. Lett. B **714**, 85 (2012), arXiv:1203.2547.
- [2] H. Bhang et al., Phys. Rev. Lett. **81**, 4321 (1998).
- [3] R. J. Prem and P. H. Steinberg, Phys. Rev. **136**, B1803 (1964).
- [4] R. E. Phillips and J. Schneps, Phys. Rev. **180**, 1307 (1969).
- [5] Y. W. Kang, N. Kwak, J. Schneps, and P. A. Smith, Phys. Rev. **139**, B401 (1965).
- [6] G. Bohm et al., Nucl. Phys. B **23**, 93 (1970).
- [7] S. Acharya et al. (ALICE), Phys. Lett. B **797**, 134905 (2019), arXiv:1907.06906.
- [8] J. Adam et al. (ALICE), Phys. Lett. B **754**, 360 (2016), arXiv:1506.08453.
- [9] C. Rappold et al., Nucl. Phys. A **913**, 170 (2013), arXiv:1305.4871.
- [10] B. I. Abelev et al. (STAR), Science **328**, 58 (2010), arXiv:1003.2030.
- [11] L. Adamczyk et al. (STAR), Phys. Rev. C **97**, 054909 (2018), arXiv:1710.00436.
- [12] E. Oset and A. Ramos, Prog. Part. Nucl. Phys. **41**, 191 (1998), nucl-th/9807018.
- [13] M. Juric et al., Nucl. Phys. B **52**, 1 (1973).
- [14] J. Adam et al. (STAR), Nature Phys. **16**, 409 (2020), arXiv:1904.10520.
- [15] A. Pérez-Obiol, D. Gazda, E. Friedman, and A. Gal, Phys. Lett. B **811**, 135916 (2020), arXiv:2006.16718.
- [16] A. Andronic, P. Braun-Munzinger, J. Stachel, and H. Stocker, Phys. Lett. B **697**, 203 (2011), arXiv:1010.2995.
- [17] R. Scheibl and U. W. Heinz, Phys. Rev. C **59**, 1585 (1999), nucl-th/9809092.
- [18] A. S. Botvina et al., Phys. Rev. C **84**, 064904 (2011), arXiv:1105.1341.
- [19] A. Andronic, P. Braun-Munzinger, and J. Stachel, Nucl. Phys. A **772**, 167 (2006), nucl-th/0511071.
- [20] C. Rappold et al., Phys. Lett. B **747**, 129 (2015).
- [21] J. Chen, D. Keane, Y.-G. Ma, A. Tang, and Z. Xu, Phys. Rept. **760**, 1 (2018), arXiv:1808.09619.
- [22] C. A. Whitten (STAR), AIP Conf. Proc. **980**, 390 (2008).
- [23] W. J. Llope (for STAR), Nucl. Instrum. Meth. A **661**, S110 (2012).
- [24] M. Anderson et al., Nucl. Instrum. Meth. A **499**, 659 (2003), nucl-ex/0301015.
- [25] M. Abdallah et al. (STAR) (2021), arXiv:2108.00924.
- [26] M. Zyzak et al. (2013), The KFPARTICLE package for the fast particle reconstruction in ALICE and CBM. Verhandlungen der Deutschen Physikalischen Gesellschaft.
- [27] R. Brun et al. (1987), CERN-DD-EE-84-1.

- [28] G. Keyes et al., Nucl. Phys. **B67**, 269 (1973).
- [29] G. Keyes et al., Phys. Rev. **D1**, 66 (1970).
- [30] G. Bohm et al., Nucl. Phys. **B16**, 46 (1970), [Erratum ibid 16 (1970) 523].
- [31] G. Keyes et al., Phys. Rev. Lett. **20**, 819 (1968).
- [32] S. A. Avramenko et al., Nucl. Phys. A **547**, 95 (1992).
- [33] H. Ota et al., Nucl. Phys. A **585**, 109 (1995).
- [34] N. Crayton et al. (1962), pp. 460–462, Proceedings of 11th International Conference on High-energy Physics.
- [35] F. Hildenbrand and H. W. Hammer, Phys. Rev. C **102**, 064002 (2020), arXiv:2007.10122.
- [36] M. Rayet and R. H. Dalitz, Nuovo Cim. A **46**, 786 (1966).
- [37] J. G. Congleton, J. Phys. G **18**, 339 (1992).
- [38] H. Kamada et al., Phys. Rev. C **57**, 1595 (1998), nucl-th/9709035.
- [39] A. Gal and H. Garcilazo, Phys. Lett. B **791**, 48 (2019), arXiv:1811.03842.
- [40] A. Gal, SQM2021 Proceedings (2021), arXiv:2108.10179.
- [41] P. Zyla et al. (Particle Data Group), Prog. Theor. Exp. Phys. **2020**, 083C01 (2020).
- [42] J. Cohen, Phys. Rev. C **42**, 2724 (1990).
- [43] H. Ota et al., Nucl. Phys. A **639**, 251c (1998).
- [44] J. D. Parker et al., Phys. Rev. C **76**, 035501 (2007), [Erratum-ibid. 76, 039904 (2007)].
- [45] B. I. Abelev et al. (STAR), Phys. Rev. C **79**, 034909 (2009), arXiv:0808.2041.
- [46] V. L. Lyuboshitz and V. V. Lyuboshitz, Phys. Atom. Nucl. **70**, 1617 (2007).
- [47] P. Liu, J. Chen, D. Keane, Z. Xu, and Y.-G. Ma, Chin. Phys. C **43**, 124001 (2019), arXiv:1908.03134.
- [48] Y. Nara, N. Otuka, A. Ohnishi, K. Niita, and S. Chiba, Phys. Rev. C **61**, 024901 (1999).
- [49] H. Liu, D. Zhang, S. He, K.-j. Sun, N. Yu, and X. Luo, Phys. Lett. B **805**, 135452 (2020), arXiv:1909.09304.
- [50] A. Andronic et al., Phys. Lett. B **697**, 203 (2011), arXiv:1010.2995 (update, preliminary).
- [51] S. Gläsel et al. (2021), arXiv:2106.14839.
- [52] V. Kireyeu et al., Bull. Russ. Acad. Sci. Phys. **84**, 957 (2020), arXiv:1911.09496.

Measurements of ${}^3_{\Lambda}\text{H}$ and ${}^4_{\Lambda}\text{H}$ Lifetime and Yield in Au+Au Collisions in the High Baryon Density Region: Supplementary Material

ADDITIONAL INFORMATION ON THE ${}^3_{\Lambda}\text{H}$, ${}^4_{\Lambda}\text{H}$ LIFETIME ANALYSIS

The main text describes the lifetime analysis using the $\sqrt{s_{\text{NN}}} = 3.0$ GeV data set. The $\sqrt{s_{\text{NN}}} = 7.2$ GeV analysis is similar, despite the difference in acceptance in the center-of-mass frame. Figure 1 shows the p_T as a function of y for reconstructed ${}^3_{\Lambda}\text{H}$ and ${}^4_{\Lambda}\text{H}$ candidates using the $\sqrt{s_{\text{NN}}} = 7.2$ GeV data set. The mid-rapidity region ($|y| < 0.5$) is not covered for this data set.

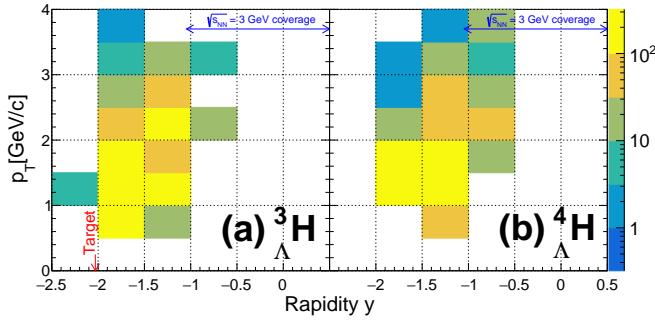


FIG. 1: The transverse momentum (p_T) versus the rapidity (y) for reconstructed (a) ${}^3_{\Lambda}\text{H}$ and (b) ${}^4_{\Lambda}\text{H}$. The target is located at the $y = -2.03$.

As in the $\sqrt{s_{\text{NN}}} = 3.0$ GeV analysis, signal counts are extracted as a function of $L/\beta\gamma$ and corrected for efficiency using GEANT simulations. Fig. 2 shows the corrected yield normalized by the total yield as a function of $L/\beta\gamma$ for ${}^3_{\Lambda}\text{H}$ and ${}^4_{\Lambda}\text{H}$ candidates. The yields from the $\sqrt{s_{\text{NN}}} = 3.0$ GeV analysis are shown for comparison. The normalized yields for the two data sets are consistent with each other.

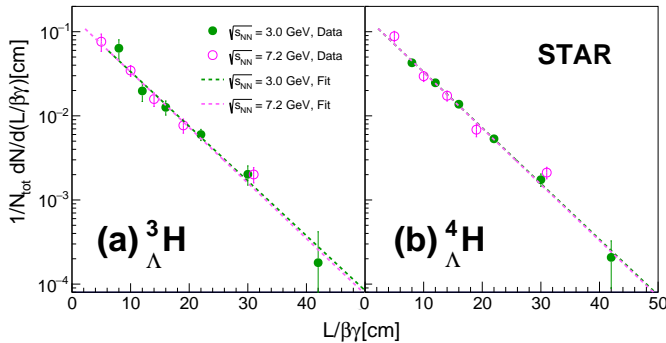


FIG. 2: The corrected yield normalized by the total yield versus $L/\beta\gamma$ for (a) ${}^3_{\Lambda}\text{H}$ and (b) ${}^4_{\Lambda}\text{H}$. The colored lines represent separate fits to the two data sets.

The yields are fitted with exponential functions to extract the lifetime. The systematic uncertainty analysis for the $\sqrt{s_{\text{NN}}} = 7.2$ GeV data set is identical to that for the $\sqrt{s_{\text{NN}}} = 3.0$ GeV data set, as described in the main text. A breakdown of the systematic uncertainties for $\sqrt{s_{\text{NN}}} = 7.2$ GeV analysis is shown in Table I.

Source	Lifetime	
	${}^3_{\Lambda}\text{H}$	${}^4_{\Lambda}\text{H}$
Analysis cuts	6.5%	4.4%
Input MC	3.4%	1.2%
Tracking efficiency	2.1%	1.8%
Signal extraction	3.8%	5.4%
Detector material	< 1%	< 1%
Total	8.5%	7.3%

TABLE I: Summary of systematic uncertainties for the lifetime measurements using $\sqrt{s_{\text{NN}}} = 7.2$ GeV data.

The lifetimes $219 \pm 20(\text{stat.}) \pm 19(\text{syst.})$ ps for ${}^3_{\Lambda}\text{H}$ and $217 \pm 16(\text{stat.}) \pm 16(\text{syst.})$ ps for ${}^4_{\Lambda}\text{H}$ are obtained from $\sqrt{s_{\text{NN}}} = 7.2$ GeV data, while the results using the $\sqrt{s_{\text{NN}}} = 3.0$ GeV data are $223 \pm 23(\text{stat.}) \pm 18(\text{syst.})$ ps for ${}^3_{\Lambda}\text{H}$ and $218 \pm 7(\text{stat.}) \pm 13(\text{syst.})$ ps for ${}^4_{\Lambda}\text{H}$. The two results are consistent with each other. Since hypernuclei lifetimes are intrinsic properties and independent of collision systems, we can combine the results by taking a weighted average $\bar{\tau}$ as follows:

$$\bar{\tau} = \frac{\sum_i w_i \tau_i}{\sum_i w_i}, \quad (1)$$

$$\sigma_{\bar{\tau}, \text{stat}} = \frac{1}{\sqrt{\sum_i w_i}}, \quad (2)$$

$$\sigma_{\bar{\tau}, \text{syst}} = \frac{\sum_i w_i \sigma_{i, \text{syst}}}{\sqrt{\sum_i w_i}}, \quad (3)$$

$$(4)$$

where τ_i is the lifetime measured at energy i , $\sigma_{i, \text{stat}}$ and $\sigma_{i, \text{syst}}$ are the statistical and systematic uncertainties of the individual measurements, and $w_i = 1/\sigma_{i, \text{stat}}^2$. Here, we assumed systematic uncertainties are fully correlated between the two measurements. The weighted averages are $221 \pm 15(\text{stat.}) \pm 19(\text{syst.})$ ps for ${}^3_{\Lambda}\text{H}$ and $218 \pm 6(\text{stat.}) \pm 13(\text{syst.})$ ps for ${}^4_{\Lambda}\text{H}$, as reported in the main text.

ADDITIONAL INFORMATION ON THE Λ LIFETIME ANALYSIS

To ensure the robustness of our ${}^3_{\Lambda}\text{H}$ and ${}^4_{\Lambda}\text{H}$ lifetime analysis, we carried out the same analysis for the Λ hy-

peron using the $\sqrt{s_{NN}} = 3.0$ GeV data. As in hypernuclei analysis, signal counts are extracted as a function of $L/\beta\gamma$ and corrected for efficiency using GEANT simulations. The corrected yield normalized by the total yield as a function of $L/\beta\gamma$ is shown in Fig. 3.

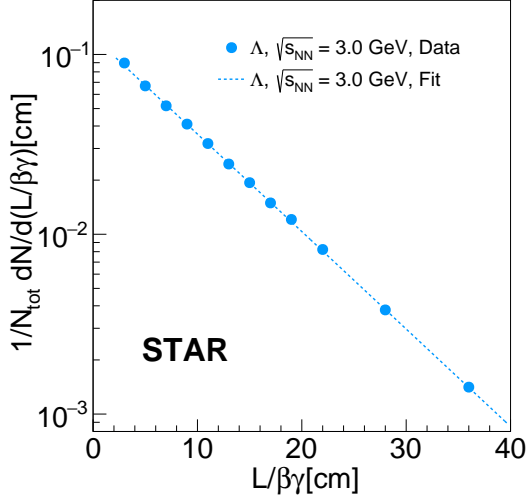


FIG. 3: The corrected yield normalized by the total yield versus $L/\beta\gamma$ for Λ at $\sqrt{s_{NN}} = 3$ GeV.

The same systematic uncertainties sources considered for hypernuclei analysis are considered for the Λ analysis. A breakdown of the systematic uncertainties is shown in Tab. II.

Source	Lifetime Λ
Analysis cuts	0.7%
Input MC	1.4%
Tracking efficiency	0.4%
Signal extraction	< 0.1%
Detector material	< 0.1%
Total	1.6%

TABLE II: Summary of systematic uncertainties for the Λ lifetime measurement using $\sqrt{s_{NN}} = 3.0$ GeV data.

The resulting Λ lifetime is $267 \pm 1(\text{stat.}) \pm 4(\text{syst.})$ ps, consistent with the PDG value [1], 263 ± 2 ps.

ADDITIONAL INFORMATION ON THE ${}^3_{\Lambda}\text{H}$, ${}^4_{\Lambda}\text{H}$ dN/dy ANALYSIS

Fig. 4 shows the corrected ${}^3_{\Lambda}\text{H}$ and ${}^4_{\Lambda}\text{H}$ invariant yields as a function of p_T for various rapidity ranges in 0–10% and 10–40% centrality Au+Au collisions at $\sqrt{s_{NN}} = 3.0$ GeV. The ${}^3_{\Lambda}\text{H}$ and ${}^4_{\Lambda}\text{H}$ in certain rapidity intervals are scaled by arbitrary factors for visibility. Dashed lines represent fits to the data using the m_T -exponential func-

tion, which are one of the functions used to extrapolate to the unmeasured p_T region.

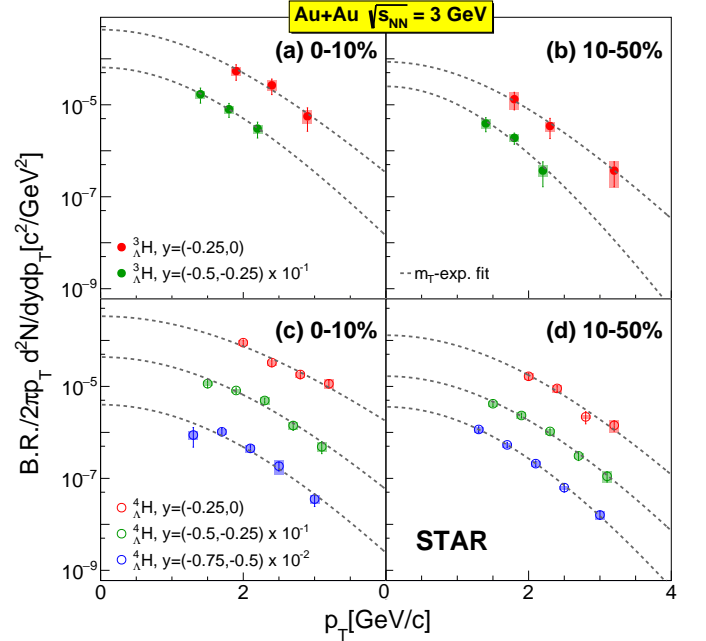


FIG. 4: (a) ${}^3_{\Lambda}\text{H}$ and (b) ${}^4_{\Lambda}\text{H}$ invariant yields as a function of p_T for various rapidity regions in 0–10% and 10–40% centrality Au+Au collisions at $\sqrt{s_{NN}} = 3.0$ GeV. Vertical lines represent statistical uncertainties, while boxes represent systematic uncertainties. The dashed black lines represent m_T -exponential function fits to the measured data points.

To estimate systematic uncertainties, the following functions are considered for extrapolation:

$$\begin{aligned}
 m_T - \text{exponential} &: \frac{dN}{m_T dm_T} \propto \exp(-m_T/T_{m_T}), \\
 p_T - \text{Gaussian} &: \frac{dN}{p_T dp_T} \propto \exp(-p_T^2/T_{p_T}^2), \\
 p_T^{1.5} - \text{exponential} &: \frac{dN}{p_T dp_T} \propto \exp(-p_T^{1.5}/T_{p_T}^{1.5}), \\
 \text{Boltzmann} &: \frac{dN}{m_T dm_T} \propto m_T \exp(-m_T/T_B),
 \end{aligned} \tag{5}$$

where T_{m_T} , T_{p_T} , and T_B are fit parameters. The m_T -exponential function is taken to be the default function, and the systematic uncertainty is taken to be the maximum difference between the result using the default function and that using other functions.

[1] P. Zyla et al. (Particle Data Group), Prog. Theor. Exp. Phys. **2020**, 083C01 (2020).